# Microphase separation in multigraft copolymer melts studied by random-phase approximation and self-consistent field theory

Cite as: J. Chem. Phys. **129**, 114905 (2008); https://doi.org/10.1063/1.2980052
Submitted: 12 June 2008 . Accepted: 18 August 2008 . Published Online: 19 September 2008

**Liquan Wang, Liangshun Zhang, and Jiaping Lin**

# Microphase separation in multigraft copolymer melts studied by random-phase approximation and self-consistent field theory

Liquan Wang, Liangshun Zhang, and Jiaping Lin[a)]
*Key Laboratory for Ultrafine Materials of Ministry of Education, School of Materials Science and Engineering, East China University of Science and Technology, Shanghai 200237, People's Republic of China*

(Received 12 June 2008; accepted 18 August 2008; published online 19 September 2008)

Microphase separation of *AB* multigraft copolymers with various numbers of graft arms per junction along the backbone was examined by the random-phase approximation and real-space implemented self-consistent field theory. The calculations carried out show that the number of graft arms per junction exerts a marked effect on the phase behavior of the multigraft copolymers. The spinodal shows an upward shift with increasing number of graft arms per junction. The order-order transitions shift toward the higher volume fraction of backbone and the ordered region becomes narrower when the number of graft arms per junction increases. The influence of the number of graft arms per junction on the domain size and the interfacial width has also been examined. It was found that the characteristic domain size decreases and the interfacial width broadens with increasing number of graft arms per junction. The theoretical results at a strong segregation were compared with the existing experimental observations and a good agreement is shown. © *2008 American Institute of Physics*. [DOI: 10.1063/1.2980052]

## INTRODUCTION

The ability of copolymer melts to self-assemble into intriguing ordered microstructures has received considerable attention.[1–5] Due to the ongoing interest in such ordered microstructures, well-defined nonlinear copolymers with complex architectures such as graft, starblock, miktoarm, and hyperbranched copolymers have been studied experimentally.[6–8] It is shown that the molecular architecture is an important factor in determining the morphologies of the microstructures, phase behaviors, and material properties. Among these copolymers with well-defined architectures, much of experimental research has focused on the graft copolymers due to their unique material properties and technological applications.[9,10] For the graft copolymer, the number of graft arm attached to the junctions along the backbone can be greater than 1. Such graft copolymer is termed as multigraft copolymer, as illustrated in Fig. 1. Gido and co-workers synthesized a series of architecturally well-defined multigraft copolymers.[11–18] Ordered lamellar, spherical, and cylindrical morphologies were observed. It has been shown experimentally that the morphologies of multigraft copolymers and the domain spacing of their ordered structures greatly depend on the number of graft arms per junction. There is a dramatic shift in the phase boundaries of multigraft copolymers as the number of graft arms per junction changes. They also found that the number of graft arms per junction influences the mechanical properties of the multigraft copolymers. For example, the tensile strength of polystyrene-*g*-polyisoprene (PS-*g*-PI) multigraft copolymers with four graft arms per junction is about twice as that of multigraft copolymers with one graft arm per junction at similar composition of PS graft arms.

In comparison to the situation of diblock and triblock copolymers, there have been much less theoretical studies regarding the phase behaviors of multigraft copolymers. Gido and co-workers proposed a constituting block copolymer hypothesis to interpret the phase behaviors of multigraft copolymers.[13–16] It is proposed that the phase behaviors of multigraft copolymers are governed by the behavior of constituting star copolymers, which are formed by snipping the connecting blocks of backbone in half. Existing Milner's theory is used to predict the phase behavior of the constituting star copolymers.[19] It has been found that the phase behavior of multigraft copolymers is generally consistent with that of the constituting star copolymers.[11] So far, the consistent block copolymer hypothesis is an effective method to predict the phase behavior of multigraft copolymers. However, this method is limited when the placement of junction is irregular since the multigraft copolymers cannot be simply cut into constituting star copolymers. Meanwhile, Milner's calculation is only strictly applicable to a strong segregation limit. Thus, systematical theoretical studies on the phase behavior of multigraft copolymers are desired. Motivated by the novel properties of multigraft copolymers and the lack of the theoretical work, we investigate the microphase separation in melts of multigraft copolymers by adopting the random-phase approximation (RPA) method and self-consistent field theory (SCFT).

The RPA calculation of scattering function originated from de Gennes,[20,21] which can give general understanding on the order-disorder transitions (ODTs), was successfully used to determine the spinodal for multiblock copolymers,[22] mixture of block copolymers and homopolymers[23] and other

[a)]Author to whom correspondence should be addressed. Tel.: +86-21-64253370. FAX: +86-21-64253539. Electronic mail: jplinlab@online.sh.cn.

 

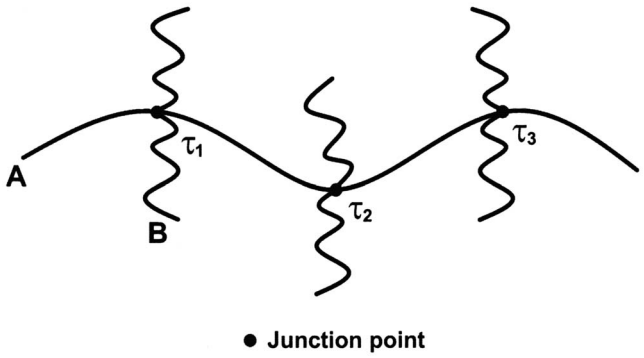


FIG. 1. Molecular architecture of the multigraft copolymer with the number of graft arms per junction $p=2$ and the number of junctions $m=3$.

complex copolymers,[24–29] etc. Shinozaki *et al.* extended this method to the comb copolymers with even or random distributions of junctions, where the number of graft arms per junction is unity.[24] They found that the spinodal of average constituting single graft copolymers determines the proximity of the ODT. Recently, Palyulin and Potemkin studied the microphase separation of *ABC* double-grafted copolymers with gradient, random, and regular sequence of junctions.[25,26] The spinodal shows a great dependence on the displacement of junctions. Although the RPA analysis can provide useful information about spinodal, more accurate numerical solutions such as self-consistent field theory (SCFT) are desired to get a complete picture of the microphase behaviors of the multigraft copolymers.

The real-space SCFT has emerged as a powerful tool to explore the phase behavior of copolymers in bulk.[30–41] Drolet and Fredrickson developed a methodology consisting of iterations of randomly generated fields at the initial step of the algorithm without a prior assumption about the mesophase symmetry.[31] Unfortunately, one major disadvantage of this method is that the algorithms locate stable and metastable states indiscriminately. One strategy for developing the most stable state SCFT solutions is to carry out the calculations by "seeding" the SCFT simulation with initial conditions that have the appropriate symmetries and by comparing the energies of the ordered structures initiated from different given configurations.[35,36] By using this strategy, Drolet and Fredrickson successfully calculated the stability of gyriod phase for diblock copolymers at strong segregation. Moreover, such a seeding procedure could dramatically reduce the computational cost of obtaining a defect-free configuration. Thus, it is feasible to study the microphase separation of multigraft copolymers in three-dimensional space by unitizing this seeding strategy. In our previous work, we used the real-space SCFT to study the bridged chain conformation characteristics of graft copolymers in bulk and aggregate morphologies of amphiphilic graft copolymers in dilute solution.[42,43] In our model, the graft copolymers exhibit two architectural parameters: the junction number and the junction position. Because of ongoing interest in novel properties of multigraft copolymers, we concentrate on the effect of the number of graft arms per junction on the phase behavior of multigraft copolymers.

In the present work, we investigate the microphase separation of multigraft copolymers with various numbers of graft arms per junction. We first determined the scattering function of multigraft copolymer melts in the disordered state and the spinodal which is the proximity of the ODT by using RPA. With the help of the information gained from RPA calculations, we then utilized real-space implemented SCFT developed by Drolet and Fredrickson to study the phase behaviors of multigraft copolymers, such as morphologies, domain spacing, and interfacial width. The phase diagrams were mapped out to show the relationship between morphologies and the number of graft arms per junction. Finally, we calculated the SCFT phase diagrams of multigraft copolymers at strong segregation to make a comparison with the existing experimental observations.

## RESULTS AND DISCUSSION

The multigraft copolymers considered in the present work are assumed to be monodispersed. The architecture of multigraft copolymers is depicted in Fig. 1. The homopolymer *B* graft arms are attached to the junction points along the homopolymer *A* backbone. The number of junctions is denoted by $m$ and the number of graft arms per junction by $p$. The $j$th junction is located at $\tau_j$ and given by $\tau_j=\tau_1+(j-1)\times(1-2\tau_1)/(m-1)$, where $1\leqslant j\leqslant m$. The degrees of polymerization of *A* and *B* chains are $N_A$ and $N_B$, respectively. Both *A* and *B* segments have the same statistical length $a$. The volume fraction of *A*-type segment is denoted by $f_A$, and thus that of *B*-type segment is $f_B=1-f_A$.

Three subsections are included in this section: "spinodal studied by RPA," "microphase behaviors studied by SCFT," and "comparison of SCFT results with experimental observations." The results in the first section are obtained from RPA described in Appendix A, and the results of the latter two sections are based on SCFT described in Appendix B. In SCFT calculations, the phase diagrams are evaluated by comparing the energies of the disordered phase and each ordered phase obtained from the calculation started from a deterministic initial condition that has symmetries of lamella ($L$), hexagonally packed cylinders ($C$), body-centered spheres ($S$), and bicontinuous gyroid ($G$) phase.

### Spinodal studied by RPA

Figure 2 illustrates influence of $p$ on spinodal of multigraft copolymers with $m=10$ and $\tau_1=0.10$. In these diagrams, the vertical axis is the segregation strength of multigraft copolymers with single junction obtained by normalizing $(\chi N)_s$ with respect to $m$, i.e. $(\chi N)_s/m$. Here, $(\chi N)_s$ is defined as the characteristic value of $\chi N$, where the magnitude of $S(\mathbf{q}*)$ diverges at the spinodal temperature. The ordered microphase-separated structures are found above the spinodal curves, while the homogeneous state is stable below the spinodal curves. From Fig. 2, it can be seen that the spinodal curves shift upward as $p$ increases, implying that the multigraft copolymers with larger $p$ are more difficult to undergo phase separation. This effect is more pronounced when the volume fraction of backbone $f_A$ is lower.

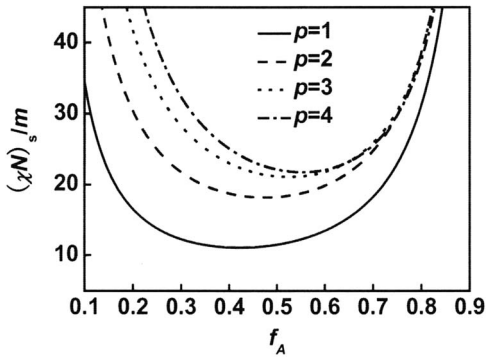


FIG. 2. Spinodal curves in $(\chi N)_s/m-f_A$ space for $AB$ multigraft copolymers with various $p$ at $m=10$ and $\tau_1=0.10$.

In addition to $f_A$, the influence of junction number $(m)$ and junction position $(\tau_1)$ on spinodal was further examined. Shown in Fig. 3(a) is a plot where $(\chi N)_s/m$ is plotted against $m$ at a given value of $\tau_1=0.15$ and $f_A=0.50$ for multigraft copolymers with various $p$. The plane of $(\chi N)_s/m$ versus $m$ includes three regions: a sharp raise at sparse junction density, a slight drop at moderate junction density, and a sharp drop at dense junction density. We note that the effect of $p$ on the spinodal at various regions displays different characters. At sparse and moderate junction density, $p$ shows a significant influence on the $(\chi N)_s/m$ of multigraft copolymer melts and the value of $(\chi N)_s/m$ increases with increasing $p$. For the multigraft copolymers with dense junction density, $p$ exerts weak impart on the spinodal curves. When $m$ is large enough, i.e., $m>40$, the spinodal curves for multigraft copolymers with various $p$ are almost identical. The influence of the variation in $\tau_1$ at a given value of $m=10$ is demonstrated in Fig. 3(b). Similarly, three regions are included: a sharp raise at smaller $\tau_1$ values, a slight drop at intermediate $\tau_1$ values, and a sharp drop at larger $\tau_1$ values. At smaller and intermediate values of $\tau_1$, $p$ has a marked effect on spinodal, and the value of $(\chi N)_s/m$ shows an increase with increasing $p$. At larger value of $\tau_1$, this effect becomes less pronounced. When $\tau_1$ is large enough, i.e., $\tau_1>0.35$, the spinodal has a weak dependence on $p$.

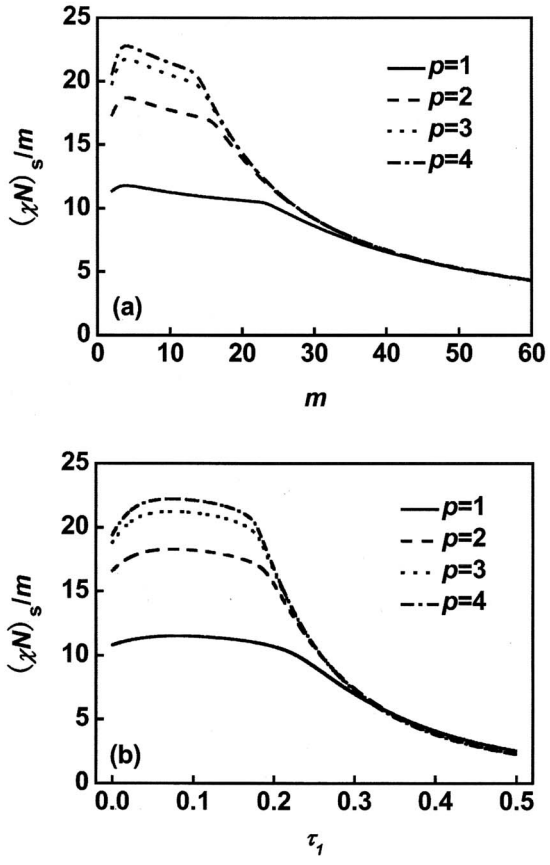


FIG. 3. (a) Spinodal curves in $(\chi N)_s/m-m$ space for $AB$ multigraft copolymers with various $p$ at $\tau_1=0.15$ and $f_A=0.50$. (b) Spinodal curves in $(\chi N)_s/m-\tau_1$ space for $AB$ multigraft copolymers with various $p$ at $m=10$ and $f_A=0.50$.

When the values of $m$ are large enough, the multigraft copolymers can be considered as the symmetric triblock copolymers containing two free end blocks and one "inner block" consisting of graft arms and a remainder backbone.[44,45] As can be seen from Fig. 3(a), the spinodal of multigraft copolymers under this condition is dependent on the volume fraction of free end blocks and inner block[46] but is very weakly dependent on $p$. As $\tau_1$ approaches 0.5, the multigraft copolymers can be regarded as the star copolymers. Under such a circumstance, $p$, which is associated with the number of arms of star copolymers, shows less pronounced effect on spinodal of multigraft copolymers [Fig. 3(b)]. It is consistent with the fact that the ODTs of star copolymers have weak dependence on the number of arms as their arm numbers are relatively larger.[47]

From the above results, we learned that the multigraft copolymers with larger $p$ are more difficult to undergo phase separation than those with smaller $p$ when $m$ and $\tau_1$ are not very large. The reason can be further understand as follows. The entropies of multigraft copolymers with different architectures in homogeneous state are nearly equal, but the entropies of multigraft copolymers with different numbers of graft arms per junction in the ordered microstructures would be different due to the fact that the graft arm blocks are pinned at the interface of ordered microstructures. As the number of graft arms per junction increases, the number of graft arm blocks confined to the interface increases. Thus, the entropy reduction associated with ODT is greater for multigraft copolymers with larger $p$. On the other hand, the transition heats for multigraft copolymers are essentially equal.[28] The greater entropy reduction for multigraft copolymers with larger $p$ requires a larger $(\chi N)_s/m$. This results in the upward shift of spinodal with increasing value of $p$.

## Microphase behaviors studied by SCFT

Figure 4 displays a series of phase diagrams in the plane of $p$ versus $f_A$ for the multigraft copolymer melts at fixed degree of segregation $\chi N/m=30.0$. As can be seen from Fig. 4, the ordered regions tend to be narrow with increasing $p$. This is in line with the fact that the multigraft copolymers with smaller $p$ are more strongly ordered than that with larger $p$ (see Fig. 2). The phase boundaries of order-order transitions (OOTs) shift towards the higher value of $f_A$ as $p$ increases. Due to the narrower ordered region and shift of OOTs as $p$ increases, the stable regions of $S_B$ become very

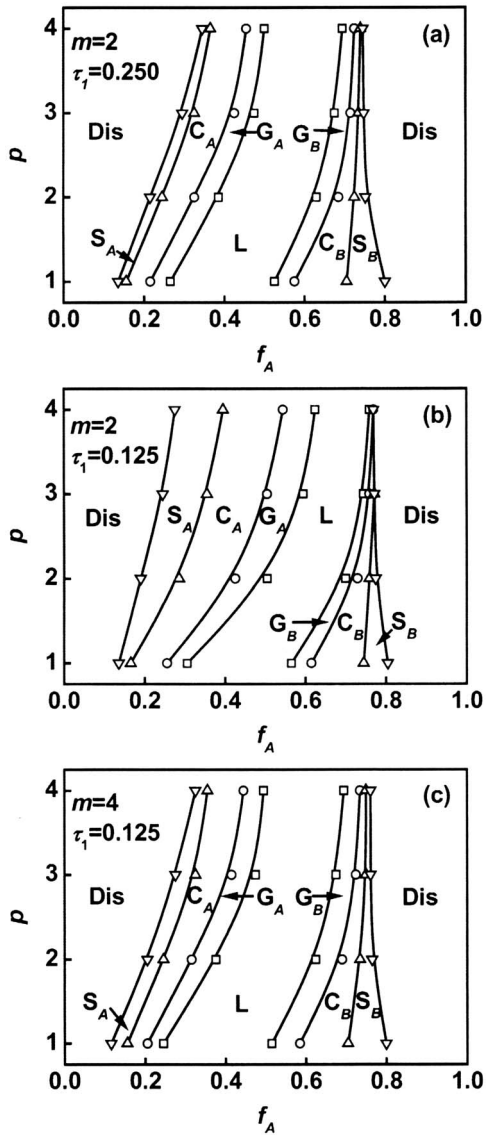


FIG. 4. Phase diagrams in $p-f_A$ space for $AB$ multigraft copolymers with (a) $m=2$ and $\tau_1=0.25$, (b) $m=2$ and $\tau_1=0.125$, and (c) $m=4$ and $\tau_1=0.125$ at $\chi N/m=30.0$. Dis labels the regions where the melt is disordered. The ordered regions are denoted as $S$ (body-centered cubic spheres), $C$ (hexagonally packed cylinders), $G$ (bicontinuous gyroid), and $L$ (lamella). The subscripts $A$ and $B$ in $C$, $S$, and $G$ denote that the minority domains of ordered structure are formed by $A$ and $B$ blocks, respectively. The hollow symbols denote the phase transitions and the solid lines are drawn to guide the eye.

narrow for the multigraft copolymers with $p=3$ and $p=4$, as shown in Fig. 4(a). With decreasing $\tau_1$ value from 0.25 to 0.125 at a given $m=2$, as shown by Figs. 4(a) and 4(b), the phase boundaries of OOTs all shift to higher values of $f_A$, while the ordered region between the ODT lines becomes broad. In addition, a more remarkable change in OOTs toward higher $f_A$ as $p$ increases is demonstrated in Fig. 4(b), which results in the disappearance of $S_B$ phase for the multigraft copolymers wifh $p=4$. As can be seen from the comparison between Figs. 4(b) and 4(c), when $m$ value increases from 2 to 4 at a given $\tau_1=0.125$, the phase boundaries of OOTs shift toward lower $f_A$ and the ordered region becomes narrow. It should be noted that the constituting star copolymers formed by snipping the midpoint of the connecting backbone blocks have the same symmetry for the cases in

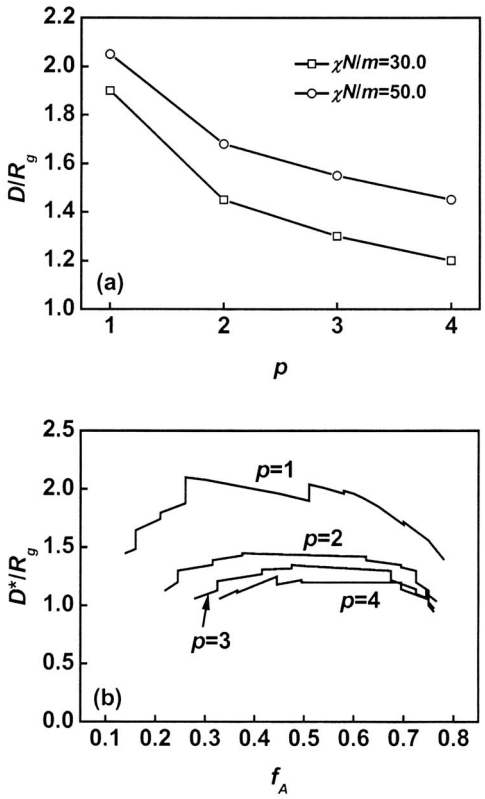


FIG. 5. (a) Lamellar period $D/R_g$ as a function of $p$ for multigraft copolymers with $f_A=0.5$, $m=4$, and $\tau_1=0.125$ at different segregation strengths $\chi N/m=30.0$ and 50.0. (b) Characteristic domain size $D^*/R_g$ plotted as a function of $f_A$ for $AB$ multigraft copolymers with various $p$ at $\chi N/m=30.0$, $m=4$, and $\tau_1=0.125$.

Figs. 4(a) and 4(c). The OOTs are nearly the same under these conditions. However, as the constituting star copolymers become more asymmetric ($\tau_1$ changes from 0.25 to 0.125 at $m=2$ or $m$ changes from 4 to 2 at $\tau_1=0.125$), shift of OOTs to higher $f_A$ is shown [Fig. 4(b)].

The behavior that the OOTs show a shift toward higher $f_A$ with increasing $p$ can be rationalized by considering the stretching energy of the multigraft copolymer chains. For the sake of argument, we consider the lamellar structure formed by the multigraft copolymers with smaller $p$. When $p$ increases, the multigraft copolymers experience a lateral crowding of the graft arms due to the fact that more graft arms accommodate on the same side of the interface in the lamellar structure. The graft arms for multigraft copolymers with larger $p$ have to be more stretched normal to the interface to fill the graft arm domain since the polymer chains must be adjusted to maintain a constant density for an incompressible system.[48] It results in the higher stretching energy of graft arm as $p$ increases. To alleviate such an effect and to lower the overall free energy, the interface curves away from the stretched graft arm domain, resulting in a preference for graft arms to reside on the convex side of the interface.[17] In this way, the graft arms find more volume close to the interface without having to stretch too much. This change in spontaneous curvature shifts the boundaries of OOTs toward the higher backbone volume fraction $f_A$ as $p$ increases.[49]

To further understand the behavior of the multigraft co-

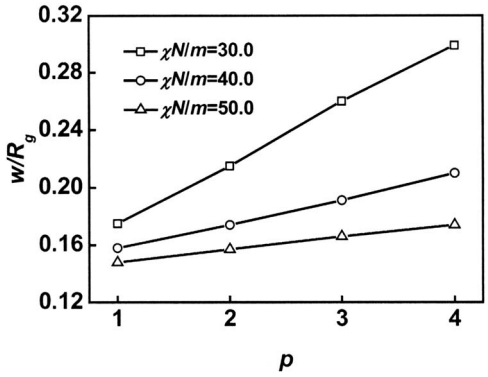


FIG. 6. Interfacial width $w/R_g$ plotted as a function of $p$ for $AB$ multigraft copolymers with $f_A=0.5$, $m=4$, and $\tau_1=0.125$ at various segregation strengths $\chi N/m=30.0$, 40.0, and 50.0.

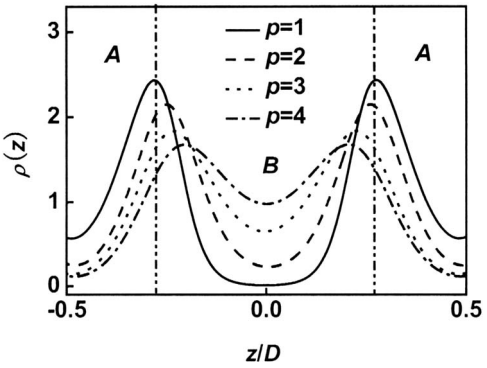


FIG. 7. Local junction distribution $\rho(z)$ for $AB$ multigraft copolymers with various $p$ at $m=4$, $\tau_1=0.125$, $f_A=0.5$, and $\chi N/m=30.0$. The coordinate $z$ normal to the lamellas is scaled by the domain spacing $D$ and the middle of $B$-rich domain occurs at $z=0$.

polymer melts, we calculated the domain size and interfacial width at $m=4$ and $\tau_1=0.125$. Figure 5(a) shows the lamellar period $D/R_g$ as a function of $p$ for multigraft copolymers at two degrees of segregation $\chi N/m=30.0$ and 50.0. The increase in the value of $p$ produces a decrease in lamellar period. This can be attributed to the fact that the graft arm chains become shorter as $p$ increases. Moreover, the lamellar period shows an increase with increasing segregation strength $\chi N/m$. The effect of variation in $p$ on the domain size is common to all morphologies. Figure 5(b) illustrates the characteristic domain size $D^*$ as a function of composition $f_A$. [$D^* \equiv 2\pi/q^*$, where $q^*$ is the principal scattering vector of given morphology. For the $L$ phase, the lamellar period is $D^*$, for the $G$ phase the size of the unit cell is $6^{1/2}D^*$, for the $C$ phase the spacing between cylinders is $(4/3)^{1/2}D^*$, and for the $S$ phase the spacing between the spheres is $(3/2)^{1/2}D^*$.][46,49] As can be seen, $D^*$ decreases as $p$ increases.

Figure 6 shows the interfacial width as a function of $p$ for lamellar phase of multigraft copolymers with $f_A=0.50$. Here, we evaluate the width as $w \equiv (d\phi_A/dz)^{-1}$ at the interface.[46] The interfacial width becomes broader as $p$ increases, implying a lower level of order in the multigraft copolymer melts with a relatively larger $p$. As $\chi N/m$ increases, the width becomes narrower in the multigraft copolymer systems. It is also noted that the effect of $p$ on the interfacial width becomes less pronounced as $\chi N/m$ increases.

The effect of variation in $p$ on the interfacial width can also be viewed from the junction distributions. Figure 7 plots the junction distributions for lamellar phase of multigraft copolymers with various $p$. The coordinate $z=0$ corresponds to the middle of $B$ graft arm domain. When $p=1$, the local volume fraction of junctions has a maximum value in the region of interface between $A$ and $B$ domains. Thus, the junctions mainly distribute at the interface. As $p$ increases, the volume fraction of junctions has an increase at the center of $B$ domain but a decrease at the interface. This suggests that the junctions delocalize from interface into $B$ graft arm domain and distribute more dispersively. The dispersive junction distribution broadens the interfacial width.

## Comparison of SCFT results with experimental observations

Some experimental results of multigraft copolymers are available in literatures for comparison with the theoretical predictions. Gido and co-workers synthesized a series of well-defined multigraft copolymers with polystyrene (PS) grafts and polyisoprene (PI) backbone (PS-$g$-PI).[11–18] The synthesized multigraft copolymers have three different numbers of graft arms per junction ($p$): $p=1$, $p=2$, and $p=4$. The microphase separation of the multigraft copolymers was investigated and three classical morphologies including lamella, cylinder, and sphere were observed. In these experiments, the morphology studies have mainly focused on PS-$g$-PI multigraft copolymers with $p=1$ and $p=2$.

In order to make a comparison with the experimental observations, we calculated the phase diagram for the multigraft copolymers at strong segregation in accord with the fact that PS and PI are strongly segregated in the experiments. Figure 8 illustrates SCFT phase diagram in $m$ versus $f_A$ plane for the multigraft copolymers with $p=1$ (a) and $p=2$ (b) at $\chi N/m=80.0$, respectively. Corresponding to the multigraft copolymers with regularly spaced junctions in the experiments, the value of $\tau_1$ was set to be $1/(m+1)$. In the present calculation, a fourth-order backward differentiation formula was employed for solution of diffusion equation [Eqs. (B3) and (B5)] in the strong segregation region. We found that the gyroid phase is stable at $\chi N/m=80.0$, although this phase has not yet been observed in the multigraft copolymer systems. The phase boundaries of OOTs show a shift toward smaller value of $f_A$ as $m$ increases. When $m$ is relatively large, this shift is very slight. The phase boundaries for different $m$ are connected by smooth lines. The morphological results obtained from the experiments of PS-$g$-PI multigraft copolymers are mapped into the SCFT phase diagrams. In the diagram, the horizontal and vertical axes correspond to the volume fraction of PI backbone and the number of junctions per molecule in the experiments, respectively. As can be seen, the SCFT calculations well reproduced the experimental results. However, some exceptions are still noted and they are denoted by filled symbols in the phase diagrams. For example, when $p=1$, the cylinder phase for multigraft copolymers with 20 vol % PI backbone are located in the gy-

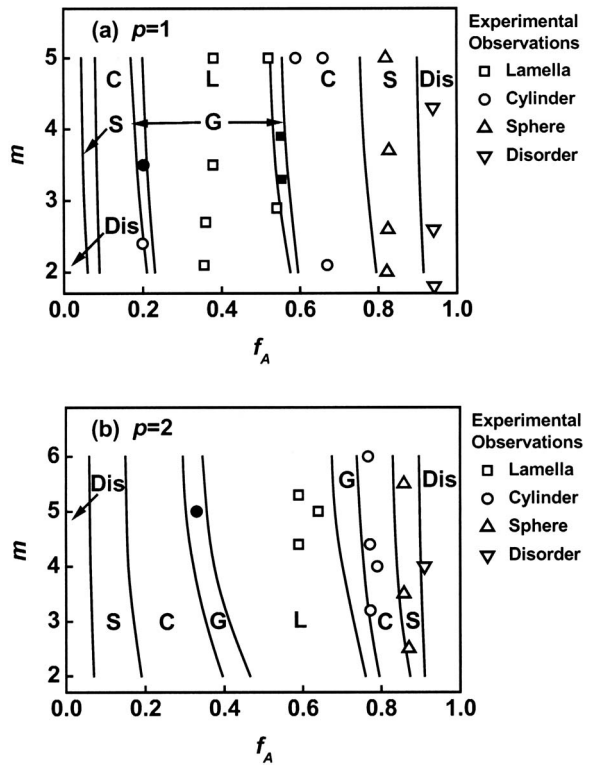


FIG. 8. Comparison of the calculated SCFT results with the experimental observations at strong segregation. Planes (a) and (b) illustrate the $m-f_A$ phase diagrams for multigraft copolymers with $p=1$ and $p=2$, respectively. Other parameters are $\tau_1=1/(m+1)$ and $\chi N/m=80.0$. The observed morphologies of polystyrene-*g*-polyisoprene multigraft copolymers are indicated by the symbols: (□) lamellar phase, (○) cylindrical phase, (△) spherical phase, and (▽) disorder state. The hollow and filled symbols show experimental observations that are consistent and inconsistent with the SCFT predicted morphologies, respectively.

roid phase of SCFT phase diagram. The common feature is that these discrepancies take place in the gyroid phase of theoretical phase diagram. In fact, the gyroid phases are absent in experiments due to the difficulty in definitively identifying the bicontinuous phases. Taking no account of the differences occurring in the gyroid phase, the SCFT results are found to be in good agreement with the experimental results. The real-space implemented SCFT is shown to be a good approach to determine the phase behavior of the multigraft copolymers.

## CONCLUSIONS

In this study, we investigated the effects of the number of graft arms per junction on the phase behaviors of multigraft copolymers using the RPA and real-space implemented SCFT. When the number of graft arms per junction $p$ increases, the spinodal of multigraft copolymers shifts upward to higher value of $(\chi N)_s/m$. Variations in the values of $m$ and $\tau_1$ can greatly change the dependence of $p$ on spinodal. When $m$ or $\tau_1$ is large enough, the variation in $p$ shows less marked effect on spinodal. By using the SCFT calculations, the phase diagrams in $p$-$f_A$ plane for multigraft copolymers were evaluated by comparing the free energy of different structures. The OOTs shift toward higher values of $f_A$ as $p$ increases. The variation in $p$ values can significantly change the domain spacing and interfacial width. The characteristic domain size shows a decrease and the interfacial width shows an increase with increasing $p$. The $m$-$f_A$ plane phase diagrams at strong segregation are also mapped out to compare with the existing experimental findings. The SCFT results can accurately capture the characteristics of the phase behaviors of multigraft copolymers.

## ACKNOWLEDGMENTS

This work was supported by National Natural Science Foundation of China (Grant Nos. 50673026 and 20574018). Supports from Doctoral Foundation of Education Ministry of China (Grant No. 20050251008), Program for New Century Excellent Talents in University in China (NCET-04-0410), and Projects of Shanghai Municipality (Nos. 06SU07002, 0652nm021, 082231, and B502) are also appreciated.

## APPENDIX A: RANDOM-PHASE APPROXIMATION

The RPA theory developed by de Gennes for binary homopolymer mixtures is a useful method in predicting thermodynamic features of block copolymer melts.[20,21] Leibler worked out RPA expansion of block copolymer melt to fourth order in the density fluctuations.[5] Because we restrict our attention to the spinodal instability, we need only to concentrate on the second-order term of the free energy expansion.[5,24] The density fluctuations in disordered state are described by density-density correlation function $S(\mathbf{q})$, which is the Fourier transform of $S(\mathbf{r})$. The RPA scattering function $S^{-1}(\mathbf{q})$ is a function of single-chain correlation functions and is written as

$$S^{-1}(\mathbf{q}) = \frac{1}{N}(F(\mathbf{q}) - 2\chi N). \tag{A1}$$

Here, $\chi$ is the Flory–Huggins parameter and $N(=N_A+mpN_B)$ denotes the total degree of polymerization of multigraft copolymers. $F(\mathbf{q})$ is given by

$$F(\mathbf{q}) = \frac{G_{AA}(\mathbf{q}) + G_{BB}(\mathbf{q}) + 2G_{AB}(\mathbf{q})}{G_{AA}(\mathbf{q})G_{BB}(\mathbf{q}) - G_{AB}^2(\mathbf{q})}, \tag{A2}$$

where $G_{AA}(\mathbf{q})$, $G_{AB}(\mathbf{q})$, and $G_{BB}(\mathbf{q})$ are the second-order correlation functions. The calculations of $G_{AA}(\mathbf{q})$, $G_{AB}(\mathbf{q})$, and $G_{BB}(\mathbf{q})$ are based on the integration over a subset of segment-segment correlation functions.[24] For the multigraft copolymers, the correlation functions are

$$G_{AA}(\mathbf{q}) = Ng(f_A,x), \tag{A3}$$

$$G_{AB}(\mathbf{q}) = 2Nmph(f_{Bt},x) \times[1-\exp(-\tau_1 f_A x)h(f_{At},mx)/h(f_{At},x)]/x, \tag{A4}$$

$$G_{BB}(\mathbf{q}) = Nmp[g(f_{Bt},x) + (p-1)h^2(f_{Bt},x) + p\exp(-f_{At}x)h^2(f_{Bt},x)u(f_{At},x)/x], \tag{A5}$$

where

$$g(f,x) = 2[fx + \exp(-fx) - 1]/x^2, \tag{A6}$$

$$h(f,x) = [1-\exp(-fx)]/x, \tag{A7}$$

$$u(f,x) = 2[h(f,x) - h(f,mx)]/h^2(f,x), \tag{A8}$$

$$f_{At} = \frac{f_A(1-2\tau_1)}{m-1}, \tag{A9}$$

$$f_{Bt} = \frac{1-f_A}{mp}, \tag{A10}$$

$$x = q^2Na^2/6 = q^2R_g^2. \tag{A11}$$

$S(\mathbf{q})$ passes through a narrow maximum at $\mathbf{q}^*$ and the magnitude of $S(\mathbf{q}^*)$ diverges at the spinodal temperature. The position of this maximum is independent of temperature ($\chi$). Thus, to find the spinodal and $\mathbf{q}^*$, we find the maximum of $S(\mathbf{q})/N$ at $\chi=0$.[24] The value of $\mathbf{q}$ at the maximum is $\mathbf{q}^*$ and the spinodal is $N/2S(\mathbf{q}^*)$. In general, the disorder-order transition occurs prior to reaching the spinodal temperature.[5,28] However, the calculation of spinodal can provide a roughly evaluation on the disorder-order transition.

## APPENDIX B: SELF-CONSISTENT FIELD THEORY

For a canonical ensemble, $n$ multigraft copolymers are contained in a system with volume $V$. Within the mean-field theory, the configuration of single copolymer chain is determined by a set of effective chemical potential fields $\omega_l(\mathbf{r})(l=A,B)$, replacing the actual interactions in the melt. The potential fields are conjugated to the density fields $\phi_l(\mathbf{r})$. We invoke an incompressibility condition ($\phi_A(\mathbf{r})+\phi_B(\mathbf{r})=1$) by introducing a Lagrange multiplier $\xi(\mathbf{r})$. For such a multigraft copolymer melt, the free energy per chain (in units of $k_BT$) is given by

$$F = -\ln\left(\frac{Q}{V}\right) + \frac{1}{V}\int d\mathbf{r}[\chi N\phi_A(\mathbf{r})\phi_B(\mathbf{r}) - \omega_A(\mathbf{r})\phi_A(\mathbf{r}) - \omega_B(\mathbf{r})\phi_B(\mathbf{r}) - \xi(1-\phi_A(\mathbf{r})-\phi_B(\mathbf{r}))], \tag{B1}$$

where $Q=\int d\mathbf{r}q_A(\mathbf{r},1)$ is the partition function of a single noninteracting grafted chain subject to the fields $\omega_A(\mathbf{r})$ and $\omega_B(\mathbf{r})$ in terms of the backbone propagator $q_A(\mathbf{r},s)$. The contour length $s$ starts from one end of the homopolymer chain ($s=0$) to the other ($s=1$). The spatial coordinate $\mathbf{r}$ is in units of $R_g$ ($R_g^2=Na^2/6$). The backbone propagator is divided into $m+1$ segments

$$q_A(\mathbf{r},s) = q_A^{(j)}(\mathbf{r},s),$$

$$\text{for } \tau_j \leqslant s < \tau_{j+1}, \quad j=0,1,\ldots,m, \quad \tau_0 \equiv 0, \quad \tau_{m+1} \equiv 1, \tag{B2}$$

where each segment satisfies the modified diffusion equation

$$\frac{N}{N_A}\frac{\partial q_A^{(j)}(\mathbf{r},s)}{\partial s} = \nabla^2 q_A^{(j)}(\mathbf{r},s) - \omega_A(\mathbf{r})q_A^{(j)}(\mathbf{r},s) \tag{B3}$$

subject to the following initial conditions:

$$q_A^{(j)}(\mathbf{r},\tau_j) = q_A^{(j-1)}(\mathbf{r},\tau_j)q_B^p(\mathbf{r},1),$$

$$j=1,2,\ldots,m, \quad q_A^{(0)}(\mathbf{r},0)=1. \tag{B4}$$

Here, $q_B(\mathbf{r},s)$ is a propagator for $B$ grafts that satisfies the modified diffusion equation

$$\frac{N}{N_B}\frac{\partial q_B(\mathbf{r},s)}{\partial s} = \nabla^2 q_B(\mathbf{r},s) - \omega_B(\mathbf{r})q_B(\mathbf{r},s) \tag{B5}$$

subject to the initial condition $q_B(\mathbf{r},0)=1$ for the free end of the graft at $s=0$. The back propagator of each $B$ graft chain attached the $j$th junction $q_{Bj}^+(\mathbf{r},s)$ satisfies Eq. (B5) and starts on the end of $B$ chain tethered to the backbone. It is therefore subject to the initial condition

$$q_{Bj}^+(\mathbf{r},0) = \frac{q_A(\mathbf{r},\tau_j)q_A(\mathbf{r},1-\tau_j)}{q_B^{p+1}(\mathbf{r},1)}. \tag{B6}$$

In terms of the single-polymer propagators, the segment densities $\phi_A(\mathbf{r})$ and $\phi_B(\mathbf{r})$ become

$$\phi_A(r) = \frac{Vf_A}{Q}\sum_{i=1}^{m+1}\int_{\tau_{i-1}}^{\tau_i} ds q_A(\mathbf{r},1-s), \tag{B7}$$

$$\phi_B(r) = \frac{Vf_B}{mQ}\sum_{j=1}^{m}\int_0^1 ds q_B(\mathbf{r},s)q_{Bj}^+(\mathbf{r},1-s). \tag{B8}$$

Finally, the minimization of free energy $F$ with respect to $\phi_A(\mathbf{r})$, $\phi_B(\mathbf{r})$, and $\xi(\mathbf{r})$ is achieved by satisfying the mean-field equations

$$\omega_A(\mathbf{r}) = \chi N\phi_B(\mathbf{r}) + \xi(\mathbf{r}), \tag{B9}$$

$$\omega_B(\mathbf{r}) = \chi N\phi_A(\mathbf{r}) + \xi(\mathbf{r}), \tag{B10}$$

$$\phi_A(\mathbf{r}) + \phi_B(\mathbf{r}) = 1. \tag{B11}$$

We can then evaluate the normalized local junction distribution

$$\rho(\mathbf{r}) = \frac{1}{m}\sum_{j=1}^{m}\rho_j(\mathbf{r}) = \frac{V}{Qm}\sum_{j=1}^{m}\frac{q_A(\mathbf{r},\tau_j)q_A(\mathbf{r},1-\tau_j)}{q_B^p(\mathbf{r},1)}, \tag{B12}$$

where $\rho_j(\mathbf{r})$ is the $j$th normalized local junction distribution.

To solve the SCFT equations, we start our calculations from two different initial states: random initial state and deterministic initial state constructed from a superposition of the leading harmonics for the microstructures. The calculation launched from a random initial state was performed in advance, which can provide insights into the unknown ordered phases and give preliminary information about the local order to initial the subsequent calculation by using the seed procedure.[36] Classic phases including the lamellar, hexagonally packed cylindrical, body-centered spherical, and bicontinuous gyriod phases are found in the calculation launched from random initial field. To accurately determine the stable state and phase boundaries, we then start calculations from a deterministic initial field constructed from functions proportional to harmonics for the structures observed form the simulations initiated form a random field configuration.[5,35,36,50] The stable structures are obtained by

exhaustively comparing the free energy of the computed structures with the free energies of three other possible structures which could exist in the melts.

For solution of the diffusion equations [Eqs. (B3) and (B5)], two formulas were employed for different segregation strengths. At weak and intermediate segregations, we utilized the Baker–Hausdorff operator splitting formula proposed by Rasmussen *et al.*[51,52] At a strong segregation, we adopted the fourth-order backward differentiation formula proposed by Cochran *et al.*[35] The densities $\phi_I(\mathbf{r})$ of special $I$, conjugated the chemical potential fields $\omega_i(\mathbf{r})$, are evaluated on Eqs. (B7)–(B10). The chemical potential fields $\omega_i(\mathbf{r})$ can be updated by using a two-step Anderson mixing scheme.[53]

All simulations were carried out in three dimensions on $32\times32\times32$ lattice with periodic boundary conditions. At intermediate segregation, contour step size $\Delta s$ for the $A$ backbone and $B$ grafts was set at 0.01, respectively. At strong segregation, $\Delta s$ was set at 0.002 for both $A$ and $B$ blocks. The numerical simulations were carried up to a convergence of $10^{-6}$ in free energy and the achievement of the incompressibility condition. We minimized the free energy with respect to the size of simulation box, as suggested by Bonbot-Raviv and Wang.[54]


[1] F. S. Bates and G. H. Fredrickson, Phys. Today **52**(2), 32 (1999).
[2] I. W. Hamley, *The Physics of Block Copolymers* (Oxford University Press, New York, 1998).
[3] M. W. Matsen and M. Schick, Phys. Rev. Lett. **72**, 2660 (1994).
[4] A. N. Semenov, Sov. Phys. JETP **61**, 733 (1985).
[5] L. Leibler, Macromolecules **13**, 1602 (1980).
[6] N. Hadjichristidis, H. Iatrou, M. Pitsikalis, and J. W. Mays, Prog. Polym. Sci. **31**, 1068 (2006).
[7] N. Hadjichristidis, H. Iatrou, M. Pitsikalis, S. Pispas, and A. Avgeropoulos, Prog. Polym. Sci. **30**, 725 (2005).
[8] N. Hadjichristidis, M. Pitsikalis, and H. Iatrou, Adv. Polym. Sci. **189**, 1 (2005).
[9] D. Gersappe, D. Irvie, A. C. Balazs, Y. Liu, J. Sokolov, M. Rafailovich, S. Schwarz, and D. G. Peiffer, Science **265**, 1072 (1994).
[10] J. P. Kennedy and J. M. Delvaux, Adv. Polym. Sci. **38**, 141 (1991).
[11] Y. Zhu, E. Burgaz, S. P. Gido, U. Staudinger, R. Weidisch, D. Uhrig, and J. W. Mays, Macromolecules **39**, 4428 (2006).
[12] R. Weidisch, S. P. Gido, D. Uhrig, H. Iatrou, J. W. Mays, and N. Hadjichristidis, Macromolecules **34**, 6333 (2001).
[13] F. L. Beyer, S. P. Gido, C. Buschl, H. Iatrou, D. Uhrig, J. W. Mays, M. Y. Chang, B. A. Garetz, N. P. Balsara, N. B. Tan, and N. Hadjichristidis, Macromolecules **33**, 2039 (2000).
[14] M. Xenidou, F. L. Beyer, N. Hadjichristidis, S. P. Gido, and N. B. Tan, Macromolecules **31**, 7659 (1998).
[15] S. P. Gido, C. Lee, D. J. Pochan, S. Pispas, J. W. Mays, and N. Hadjichristidis, Macromolecules **29**, 7022 (1996).
[16] C. Lee, S. P. Gido, Y. Poulos, N. Hadjichristidis, N. B. Tan, S. F. Trevino, and J. W. Mays, J. Chem. Phys. **107**, 6460 (1997).
[17] C. Lee, S. P. Gido, Y. Poulos, N. Hadjichristidis, N. B. Tan, S. F. Trevino, and J. W. Mays, Polymer **39**, 4631 (1998).
[18] C. Lee, S. P. Gido, M. Pitsikalis, J. W. Mays, N. B. Tan, S. F. Trevino, and N. Hadjichristidis, Macromolecules **30**, 3732 (1997).
[19] S. T. Milner, Macromolecules **27**, 2333 (1994).
[20] P. G. de Gennes, J. Phys. (Paris) **31**, 235 (1970).
[21] P. G. de Gennes, *Scaling Concepts in Polymer Physics* (Cornell University Press, Ithaca, 1979).
[22] H. Benoit and G. Hadziioannou, Macromolecules **21**, 1449 (1988).
[23] M. D. Whitmore and J. Noolandi, Macromolecules **18**, 2486 (1985).
[24] A. Shinozaki, D. Jasnow, and A. C. Balazs, Macromolecules **27**, 2496 (1994).
[25] V. V. Palyulin and I. I. Potemkin, J. Chem. Phys. **127**, 124903 (2007).
[26] V. V. Palyulin and I. I. Potemkin, Polym. Sci., Ser. A Ser. B **49**, 473 (2007).
[27] E. W. Cochran, D. C. Morse, and F. S. Bates, Macromolecules **36**, 782 (2003).
[28] M. Olvera de la Cruz and I. C. Sanchez, Macromolecules **19**, 2501 (1986).
[29] T. Hashimoto, Y. Ijichi, and L. J. Fetters, J. Chem. Phys. **89**, 2463 (1988).
[30] F. Drolet and G. H. Fredrickson, Macromolecules **34**, 5317 (2001).
[31] F. Drolet and G. H. Fredrickson, Phys. Rev. Lett. **83**, 4317 (1999).
[32] V. Ganesan and G. H. Fredrickson, Europhys. Lett. **55**, 814 (2001).
[33] G. H. Fredrickson, V. Ganesan, and F. Drolet, Macromolecules **35**, 16 (2002).
[34] D. M. Patel and G. H. Fredrickson, Phys. Rev. E **68**, 051802 (2003).
[35] E. W. Cochran, C. J. Garcia-Cervera, and G. H. Fredrickson, Macromolecules **39**, 2449 (2006).
[36] G. H. Fredrickson, *The Equilibrium Theory of Inhomogeneous Polymers* (Oxford University Press, Oxford, 2006).
[37] Y. Jiang, X. Yan, H. Liang, and A.-C. Shi, J. Phys. Chem. B **109**, 21047 (2005).
[38] P. Chen, H. Liang, and A.-C. Shi, Macromolecules **40**, 7329 (2007).
[39] L. Zhang, J. Lin, and S. Lin, Macromolecules **40**, 5582 (2007).
[40] X. Ye, T. Shi, Z. Lu, C. Zhang, Z. Sun, and L. An, Macromolecules **38**, 8853 (2005).
[41] X. Ye, X. Yu, Z. Sun, and L. An, J. Phys. Chem. B **110**, 12042 (2006).
[42] L. Zhang, J. Lin, and S. Lin, J. Phys. Chem. B **111**, 351 (2007).
[43] L. Zhang, J. Lin, and S. Lin, J. Phys. Chem. B **111**, 9209 (2007).
[44] R. J. Nap, C. Kok, G. ten Brinke, and S. I. Kuchanov, Eur. Phys. J. E **4**, 515 (2001).
[45] R. J. Nap and G. ten Brinke, Macromolecules **35**, 952 (2002).
[46] M. W. Matsen and R. B. Thompson, J. Chem. Phys. **111**, 7139 (1999).
[47] G. M. Grason and R. D. Kamien, Macromolecules **37**, 7371 (2004).
[48] D. M. Cooke and A.-C. Shi, Macromolecules **39**, 6661 (2006).
[49] M. W. Matsen, J. Chem. Phys. **113**, 5539 (2000).
[50] M. Wohlgemuth, N. Yufa, J. Hoffman, and E. L. Thomas, Macromolecules **34**, 6083 (2001).
[51] G. Tzeremes, K. Ø. Rasmussen, L. Lookman, and A. Saxena, Phys. Rev. E **65**, 041806 (2002).
[52] K. Ø. Rasmussen and G. Kalosakas, J. Polym. Sci., Part B: Polym. Phys. **40**, 1777 (2002).
[53] V. Eyert, J. Comput. Phys. **124**, 271 (1996).
[54] Y. Bohbot-Raviv and Z.-G. Wang, Phys. Rev. Lett. **85**, 3428 (2000).